Frontiers in Ecology and the Environment

Placing unprecedented recent fir growth in a European-wide and Holocene-long context

Ulf Büntgen, Willy Tegel, Jed O Kaplan, Marcus Schaub, Frank Hagedorn, Matthias Bürgi, Rudolf Brázdil, Gerhard Helle, Marco Carrer, Karl-Uwe Heussner, Jutta Hofmann, Raymond Kontic, Tomáš Kyncl, Josef Kyncl, J Julio Camarero, Willy Tinner, Jan Esper, and Andrew Liebhold

Front Ecol Environ 2013; doi:10.1890/130089

Placing unprecedented recent fir growth in a European-wide and Holocene-long context

Ulf Büntgen[1,2,3*], Willy Tegel[4], Jed O Kaplan[5], Marcus Schaub[1], Frank Hagedorn[1], Matthias Bürgi[1], Rudolf Brázdil[3,6], Gerhard Helle[7], Marco Carrer[8], Karl-Uwe Heussner[9], Jutta Hofmann[10], Raymond Kontic[11], Tomáš Kyncl[12], Josef Kyncl[12], J Julio Camarero[13,14], Willy Tinner[2,15], Jan Esper[16], and Andrew Liebhold[17]

Forest decline played a pivotal role in motivating Europe's political focus on sustainability around 35 years ago. Silver fir (*Abies alba*) exhibited particularly severe dieback in the mid-1970s, but disentangling biotic from abiotic drivers remained challenging because both spatial and temporal data were lacking. Here, we analyze 14 136 samples from living trees and historical timbers, together with 356 pollen records, to evaluate recent fir growth from a continent-wide and Holocene-long perspective. Land use and climate change influenced forest growth over the past millennium, whereas anthropogenic emissions of acidic sulfates and nitrates became important after about 1850. Pollution control since the 1980s, together with a warmer but not drier climate, have facilitated an unprecedented surge in productivity across Central European fir stands. Restricted fir distribution prior to the Mesolithic and again in the Modern Era, separated by a peak in abundance during the Bronze Age, is indicative of the long-term interplay of changing temperatures, shifts in the hydrological cycle, and human impacts that have shaped forest structure and productivity.

Front Ecol Environ 2013; doi:10.1890/130089

Environmental political action catalyzed about 35 years ago in Europe, with the widespread public perception that forests were dying as a result of air pollution and related acid deposition (Schütt and Cowling 1985; Innes 1987; Kandler and Innes 1995). This apparent decline, considered to be unprecedented in a broad spatiotemporal context, stimulated new pollution control legislation and promoted environmental awareness. However, scientific curiosity about this subject gradually waned after a decade of intensive research in conjunction with evidence of forest ecosystem recovery (Spiecker 1995).

Reports of crown dieback and declining tree growth during the mid-1970s were mostly derived from individual stands of silver fir (*Abies alba*; Kandler and Innes 1995). These changes were linked with local to regional assessments of sulfur emissions, drought, insect and pathogen outbreaks, and soil acidification. However, quantifying and fully understanding the reasons for these variations in forest health were complicated by a general lack of long and well replicated tree-ring width chronologies (ie annually resolved and properly dated time series of radial stem thickening) and the difficulty of disentangling the biotic and abiotic factors that might be responsible for the observed changes. In other analyses of environmental change, chronologies of tree-ring width have been extremely useful in characterizing long-term variability in climatological and ecological conditions and the effects on forest productivity and vigor (Büntgen *et al.* 2011b, 2013). Unfortunately, extensive temporal and spatial datasets on silver fir growth have not been available and this has limited the opportunities for understanding past changes in the species' growing conditions across Europe.

Here, we compile ring-width measurements from living fir trees and historical construction timbers throughout Europe and use them to quantify trends in forest productivity over the past millennium. We also utilize paleobotanical pollen profiles to reconstruct trends in fir land cover over the entire Holocene. This novel, multi-proxy (tree-ring/pollen) approach provides a much broader and longer term perspective on the highly publicized Central European forest decline of the 1970s and therefore allows for an improved understanding of the external drivers of fir growth and abundance at various spatiotemporal scales.

Methods

Core and disc samples of 14 136 living and historical silver fir trees were collected over the past four decades in Spain, France, Italy, Switzerland, Germany, Poland, Slovakia, Ukraine, and the Czech Republic. All historical samples were obtained from construction timbers that made up the frameworks of roofs and walls in old buildings. Such materials represent a rich source for dendrochronological studies, providing data that go back to medieval times across most of Central Europe (WebFigure 1). (See Büntgen *et al.* [2011b, 2013] for a more detailed description of the various tree-ring archives that offer a unique source of multi-centennial to millennial-long tree-ring chronologies in Central Europe.)

[1]*Swiss Federal Research Institute WSL, Birmensdorf, Switzerland *(buentgen@wsl.ch);* [2]*Oeschger Centre for Climate Change Research, Bern, Switzerland;* [3]*Global Change Research Centre AS CR, Brno, Czech Republic;* [4]*Institute for Forest Growth IWW, University of Freiburg, Freiburg, Germany;* *continued on last page*

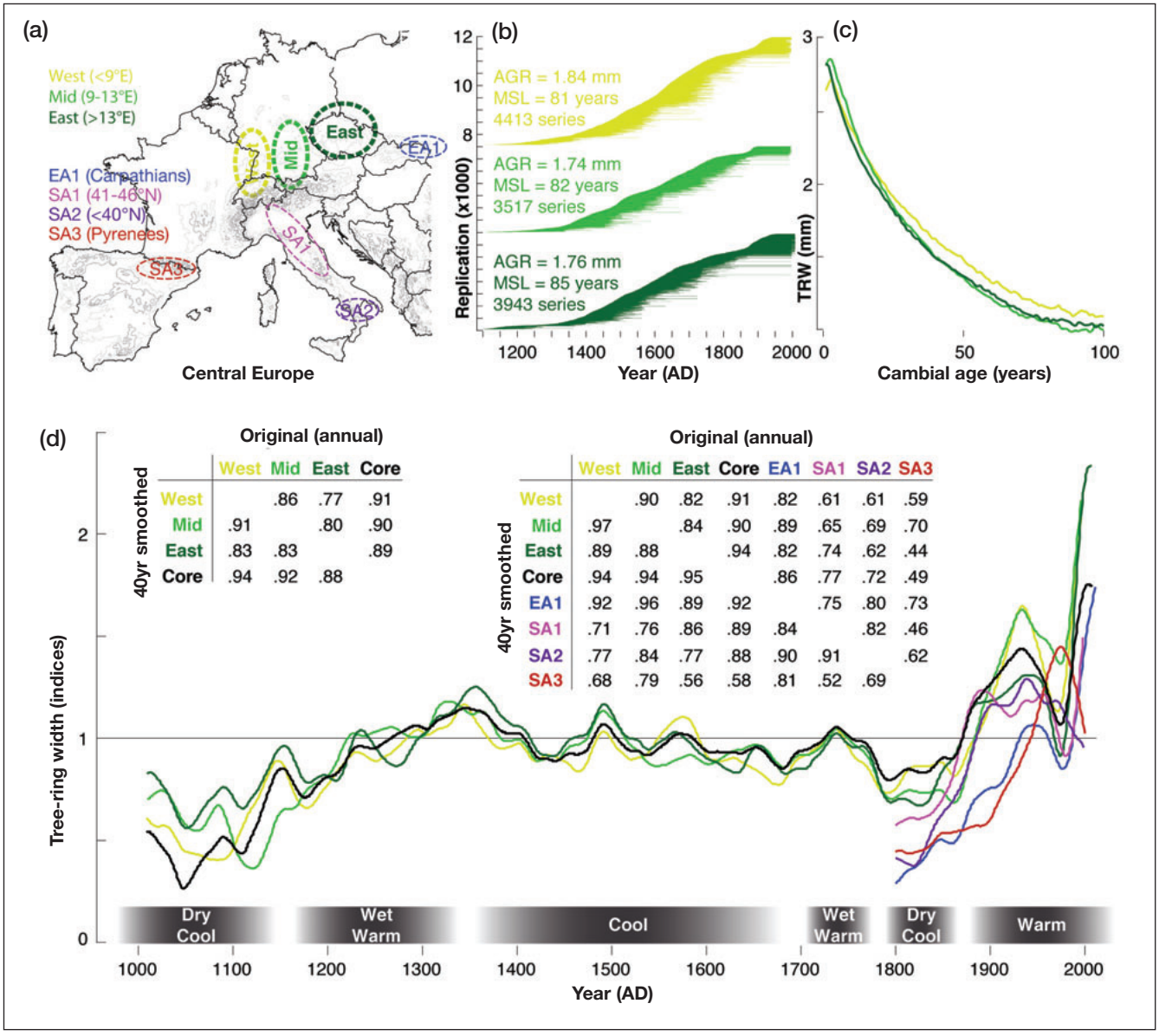

40yr smoothed	West	Mid	East	Core
West		.86	.77	.91
Mid	.91		.80	.90
East	.83	.83		.89
Core	.94	.92	.88	

Original (annual)

40yr smoothed	West	Mid	East	Core	EA1	SA1	SA2	SA3
West		.90	.82	.91	.82	.61	.61	.59
Mid	.97		.84	.90	.89	.65	.69	.70
East	.89	.88		.94	.82	.74	.62	.44
Core	.94	.94	.95		.86	.77	.72	.49
EA1	.92	.96	.89	.92		.75	.80	.73
SA1	.71	.76	.86	.89	.84		.82	.46
SA2	.77	.84	.77	.88	.90	.91		.62
SA3	.68	.79	.56	.58	.81	.52	.69	

Figure 1. *(a) Location of the three core regions of living and historical silver fir sampling that are situated north of the Alpine Arc (West, Mid, and East), as well as the additional four sampling areas near the species-specific distribution limits in the Carpathian Arc (EA1), along the Italian Peninsula (SA1 and SA2), and in the Pyrenees Mountains (SA3). (b) Temporal distribution of the 11 873 living and historical fir samples (ie measurement series) from the three core regions, along with information on average growth rate (AGR), mean segment length (MSL), and sample replication. (c) The biological aging trends expressed by the Regional Curve (RC) per region (West, Mid, and East), which shows exponentially decreasing tree-ring widths (TRWs along the y axis) with increasing tree age (years along the x axis). (d) Regional subset chronologies of the three fir core subsets (green), their mean values (black), and the four more marginal chronologies (blue–red). All chronologies were RCS detrended and additionally smoothed with a 40-year low-pass filter. Highly significant correlation coefficients ($P < 0.00001$ in all cases) of the original (upper right values) and 40-year smoothed (lower left values) chronologies from the three core regions (West, Mid, and East) were computed over the 1133–1996 common period, during which each chronology is replicated by at least 20 series. Additional correlation coefficients, calculated between all core and marginal chronologies over the 1800–1996 industrial period, were also significant ($P < 0.0001$). The gray horizontal bar at the bottom refers to general Central European climate conditions, as introduced by Büntgen* et al. *(2011b).*

Our compilation of annual-ring-width data spans 962–2011 CE and covers the entire range of silver fir distribution, including three core regions north of the European Alps (West, Mid, and East), as well as fringes in the Carpathian Arc (EA1), northern and southern Italy (SA1 and SA2), and the Pyrenees (SA3) (Figure 1a; WebFigure 1; WebTable 1). This represents the world's largest dendrochronological dataset for a single conifer species. Samples from the three core regions were exclusively taken from forest stands < 900 m above sea level (asl), and each contains sequences of at least 50 consecutive rings (Büntgen *et al.* 2011a, 2012b). Sample sizes,

aging trends, and growth levels are similar among the core regions (Figure 1, b–d), with significant correlations ($r_{1133–1996}$ = 0.77–0.94; $P < 0.00001$), indicating highly synchronized growth behavior. The massively replicated core subsets of 3517–4413 samples each share a high degree of common growth variability (ie internal signal strength; WebFigures 2 and 3). See also Büntgen *et al.* (2011a, 2012b) for additional information on growth trends and levels among the different regions (WebFigure 2, 3, 4).

Geographically averaged instrumental measurements were extracted from a network of meteorological stations across the greater Alpine region (HISTALP; Auer *et al.* 2007). These records were used to assess changes in the relationship between radial fir growth and monthly temperature means (since 1760 CE), sunshine duration (since 1880), precipitation totals (since 1800), and cloudiness (since 1840). A suite of 2736 correlation coefficients, together with split-period and moving-window approaches, were applied to detect spatiotemporal instability in the relationship between Central European fir growth and climate variation.

Pre-instrumental indices of temperature and precipitation back to 1500 CE were further derived from documentary evidence, including annals; chronicles; memorial books; visual daily weather observations; private correspondence; illustrated broadsheets; newspapers and journals; pictorial evidence; stall-keepers' and market songs; early scientific papers and communications; epigraphic sources; and early instrumental meteorological measurements (Brázdil *et al.* 2005). Central European temperature indices were obtained from Dobrovolný *et al.* (2010), while corresponding precipitation indices were compiled specifically for this study. These data were used to explore associations of annual weather conditions with regional- to continental-scale extremes in radial growth of the silver fir. Individual months were classified on an ordinal scale: –3 (extremely cold/dry), –2 (very cold/dry), –1 (cold/dry), 0 (normal), +1 (warm/wet), +2 (very warm/wet), and +3 (extremely warm/wet), with seasonal indices fluctuating from –9 to +9 (WebTable 2; see also Dobrovolný *et al.* [2010] and Büntgen *et al.* [2011a] for details).

We used decadal records of sulfur dioxide (SO_2) and nitrogen oxide (NO_x) emissions across Europe, extracted from version 2.0 of the Emission Database for Global Atmospheric Research (EDGAR 2.0; van Aardenne *et al.* 2001), to explore their possible associations with fir growth and vigor back to 1850 CE.

Paleoecological evidence of silver fir occurrence was synthesized from the European Pollen Database (Fyfe *et al.* 2009), the PANGAEA database (www.pangaea.de), values digitized from published pollen diagrams, and personal communications from specific authors (WebTable 3). These pollen records were derived from sediment cores of European lakes, swamps, and bogs. *Abies* pollen cannot be differentiated at the species level, so records were made at the genus level. The percentage of pollen that was composed of fir pollen at each sampling site was binned into multiple 500-year periods spanning the past 10 500 years. Using a 3D thin plate spline method that uses elevation as a third dimension (Collins *et al.* 2012), we spatially interpolated these values on five arc minute (~5 km) grid cells. The resulting time sequence of fir distribution maps encompassed the Holocene and was spatially adapted to cover the continent's major drainage basins north of the Alps, and from the Rhine to the Danube.

Results

Fir growth varied considerably over the past several centuries. Low growth rates occurred prior to ~1200, from ~1600 to 1700, and from 1780 to 1870, whereas anomalously high growth rates occurred at most sites ~1350, ~1490, from ~1880 to 1950, and from the mid-1980s to the present (Figure 1; WebFigure 4). Reduced fir growth rates prior to ~1200 and in the first half of the 19th century coincided with relatively dry and cold periods (Figure 1d), whereas above-average growth rates paralleled periods of an overall wetter and warmer climate (Büntgen *et al.* 2011b). The relationship between tree age and growth resembles a negative exponential function, characteristic of a species regenerating under relatively open canopy forest structure (WebFigure 2). The appearance of suppressed juvenile growth prior to ~1300 and in the 19th century indicates relatively higher stand densities during these periods, which, in turn, is suggestive of greater resource competition (Büntgen *et al.* 2012b).

Growth–climate relationships of all ring-width measurement datasets from the three core regions (West, Mid, and East) remain non-significant overall ($P > 0.001$), with the exception of some spurious agreement between recently increasing trends in temperature and fir growth (Figure 2). Correlation coefficients that are based on six slightly different silver fir chronologies (ie raw measurements, raw measurements after power-transformation, Regional Curve Standardization (RCS) detrending, RCS detrending after power-transformation, negative exponential functions, and 80-year spline functions), 19 monthly and seasonal resolved targets among temperature, sunshine, precipitation, and cloudcover, two independent early and late split periods (1760–1950 and 1951–2007), and three geographical regions (Northwest Alpine Arc, Northeast Alpine Arc, and the Greater Alpine Region) accumulate to growth–climate 2736 pairings (see also Büntgen *et al.* [2012a] for methodological insight on the so-called "Ensemble Approach"). An array of statistically significant negative correlations with indices of May temperature and springtime sunshine before the mid-20th century indicate the inverse relationship of these two parameters with precipitation and therefore suggest some dependency of fir growth on soil moisture availability at the beginning of the vegetation

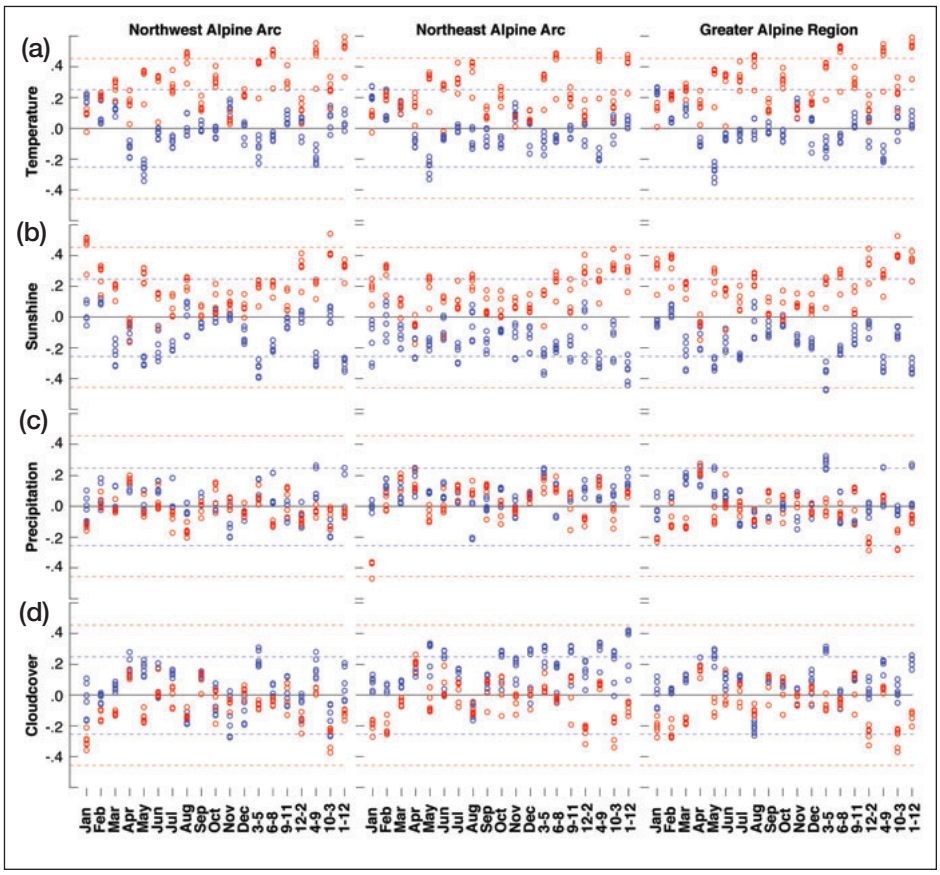

Figure 2. *A total of 2736 associations (correlation coefficients) between six slightly different silver fir chronologies and 19 monthly and seasonally resolved climatic targets were calculated over two independent early and late split periods (1760–1950 [blue] and 1951–2007 [red]) and three geographical regions (Northwest Alpine Arc, Northeast Alpine Arc, and the Greater Alpine Region) (Auer* et al. *2007). The six fir chronologies – based on raw measurements, raw measurements after power-transformation, RCS detrending, RCS detrending after power-transformation, negative exponential functions, and 80-year spline functions – were calculated from all ring-width measurement series of the three core regions (West, Mid, and East). The monthly (a) temperature, (b) precipitation, (c) sunshine, and (d) cloudcover indices range from January–December, whereas the seven climatologically defined seasonal means include March–May (3–5), June–August (6–8), September–November (9–11), December–February (12–2), April–September (4–9), October–March (10–3), and annual (1–12). Horizontal dashed lines refer to the 99.9% significance levels, independently calculated for the early and late split periods (blue and red).*

period, in line with the findings of Büntgen *et al.* (2011a). Nevertheless, a lack of short-term climate sensitivity is evident and possibly reflects transient growth responses to environmental changes, related in part to the fact that all samples from the core regions were collected at < 900 m asl. The high degree of temporal instability in the obtained growth–climate associations is further emphasized by 31-year moving correlation coefficients (WebFigure 5). Although non-significant overall, there is a tendency for increasing positive relationships between fir growth and temperature/sunshine after 1950 (although partly inflated by similar trend behavior), whereas recent correlations with precipitation/cloudcover are decreasing. We also found little similarity between reconstructed April–June precipitation totals and June–August temperature means (WebFigure 6). Nevertheless, there was clear evidence that negative and positive growth extremes have coincided with dry and humid springtime conditions, respectively, during the past 500 years (WebTable 2).

Growth rates among all regions were highly synchronized ($r_{1800–1996}$ = 0.44–0.97) and generally increased during the 1800–1996 industrial era (Figure 3a). There was a synchronous post-1950 ring-width depression, but growth strongly increased from the early 1980s onward, though this was less pronounced in Southern Italy and the Spanish Pyrenees (Figure 3b).

Postglacial forests included only a small fraction of fir trees between ~8000 and 6000 BCE (Figure 4), after which the relative amount of fir steadily increased. Despite a short depression ~4000 BCE, fir pollen continued to increase relative to total terrestrial pollen, reaching a maximum of ~7% on average ~1000 BCE, which preceded a continuous decline during the Common Era.

Discussion

During the early 1980s, considerable scientific and public attention was directed toward ongoing extensive dieback in European forest trees, especially silver fir (Schütt and Cowling 1985; Innes 1987; Kandler and Innes 1995). Concern over these declines motivated stricter air-pollution regulation and generated a new political focus on the environment that persists to this day in Europe. Although several studies documented local to regional forest declines during this period, primarily across the central portion of the continent, it is useful to revisit this dieback from a much broader perspective in time and space.

Paleobotanical evidence from pollen profiles (WebTable 3) indicates that fir trees were a fairly small component of postglacial forests from 8000 to 6000 BCE (Figure 4). Fir pollen, however, steadily increased after ~6000 BCE, both as a percentage of the total terrestrial assemblage and relative to other arboreal taxa. Range expansion and increased abundance were likely triggered

by a shift to moister conditions after the "8.2k event" (Tinner and Lotter 2006). Despite the declining total arboreal pollen percentage after ~4000 BCE, fir pollen continued to increase until ~1000 BCE, probably due to increasingly moist European conditions (Feurdean and Willis 2008). This prehistoric fir peak was followed by a continuous decline that has lasted until the present.

This long-term trend is corroborated by dendroarchaeological evidence – from several Swiss Neolithic lakeside dwellings – in the form of a vast abundance of fir wood ~3500 BCE (Figure 4). Investigations of northern Alpine settlements revealed thousands of fir logs used for Bronze Age and newer construction. Interestingly, fir wood not only dominated roof construction and skeleton framing during the past millennium but was also frequently used in assembling ancient Roman barrels, wells, and ships. However, increasing forest extraction, agricultural expansion, and competition from beech, probably diminished total silver fir cover during recent millennia. Prior to the conversion of pristine forests into fire-prone macchia-dominated ecosystems (densely growing evergreen Mediterranean-type vegetation) at ~4000–3000 BCE (Colombaroli *et al.* 2007), fir was abundant in Mediterranean coastal and hilly areas, suggesting high performance of silver fir under conditions warmer than those of today.

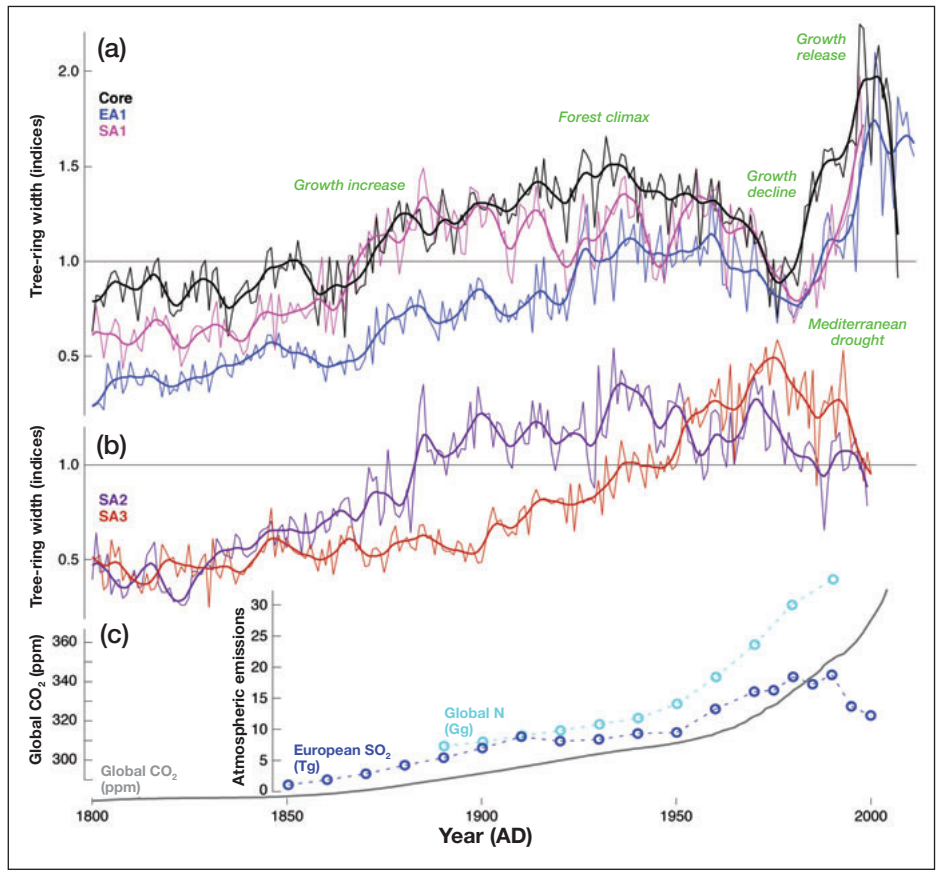

Figure 3. *Changes in annual (original unsmoothed data) and decadal (10-year low-pass filtered time series) fir growth across (a) Central Europe and (b) the Mediterranean (SA2 = Southern Italy and SA3 = Pyrenees). (c) Long-term evolution of global nitrogen (N) and atmospheric carbon dioxide (CO_2) concentrations, as well as European-scale estimates of sulfur dioxide (SO_2) emissions, which were compiled by van Aardenne* et al. *(2001).*

Timber harvesting, along with intense woodland grazing and litter collection, influenced the disproportionate decrease in fir abundance long before industrialization. Clear-cutting, as part of intensive forest extraction since the 14th century and especially after the Thirty Years' War (~1618–1648), root decay, and later smoke damage all contributed to some extent to an accelerated European-wide decline in the 17th century. Fir regeneration was suppressed by competition from spruce, beech, and pine, which were intensively planted from the 18th and early-19th century onwards, following clear-cutting (Bürgi and Schuler 2003). Exploitative land-use/land-cover changes may partially explain declining fir abundance from medieval times until ~1840.

Despite the millennium-long decline in fir populations, productivity has substantially increased Europe-wide during the past two centuries (Figure 3). This boost in productivity may be attributed in part to the advent of less intense practices of woodland utilization. However, these changes alone cannot explain the synchronous increase in productivity, because different strategies were applied at different times and at different national, county, and even communal levels. Clear-cutting after artificial spruce regeneration may have impacted the mid- and eastern core subsets in a similar manner. For example, Swiss federal laws established in 1870 banned forest grazing (to which fir is particularly sensitive), and clear-cutting was abandoned shortly after the beginning of the 20th century (Bürgi and Schuler 2003), when various forms of group cutting were promoted. Selective logging of fir was applied in the Venetian Republic of Northern Italy, and fir grazing in combination with coppicing of the broadleaf species was applied in the Italian Piedmont.

Industrialization presumably promoted fir recovery beginning around the mid-19th century, since wood fuel was gradually replaced by fossil fuels, particularly since the 1950s when globalization led to the abandonment of local semi-autarkic (ie semi-self-sufficient) agricultural production systems throughout the mountainous areas of Europe. The long-term ring-width increase that occurred from ~1840 to 1940 in almost all fir habitats across the

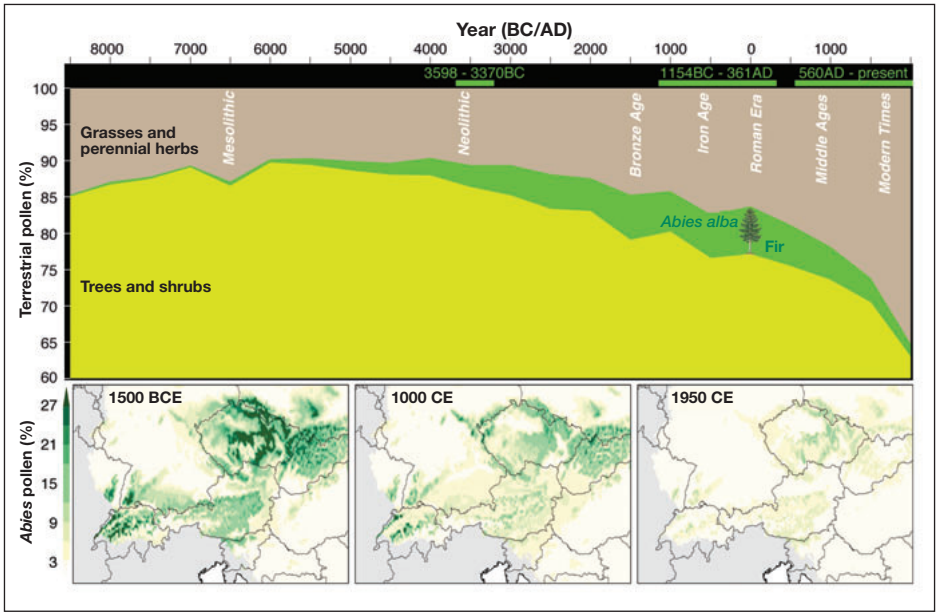

Figure 4. *Pollen-based estimates of relative changes in Central European silver fir distribution as compared with other tree and shrub species, as well as with grasses and perennial herbs during most of the Holocene (8500 BCE to 1950 CE). The relative proportion of fir abundance reveals a maximum peak between around 1500 BCE and 500 CE, after which a long-term decline in fir distribution and abundance, together with a general decrease in forest cover, stretches from medieval times to the present. The three lower maps are temporal snapshots of Central European fir distribution and abundance at 1500 BCE, 1000 CE, and 1950 CE. Green horizontal bars at the upper x axis provide the temporal distribution of dendrochronologically dated fir wood, including material from Neolithic lakeside dwellings, ancient Roman settlements, and medieval constructions in Central Europe.*

continent was therefore probably stimulated by a combination of land-use practices and warming without drying, as well as through fertilization by nitrogen (N) and carbon dioxide (CO_2) (Figure 3c; Körner 2006; Thomas *et al.* 2008). In contrast, sulfur (in the form of sulfur dioxide, SO_2) deposition caused negative feedbacks, with soil acidification inducing aluminum toxicity to fine roots (van Breemen *et al.* 1982). Rising atmospheric CO_2 concentrations from pre-industrial levels in the mid-20th century (280–320 parts per million [ppm]) potentially influenced the continental-wide growth enhancement (Körner 2006). The absolute change of ~40 ppm in atmospheric CO_2 prior to the mid-20th century possibly initiated an effect on tree growth similar to that of the most recent increase from 315–385 ppm, which was partly masked by pollutants (SO_2, NO_x) and tropospheric ozone (O_3) after ~1950, for instance.

A substantial and synchronous decline in fir productivity, despite the ongoing multi-century trend of increasing growth, is clearly evident during the 1970s, followed by a recovery phase (Figure 3a). The late-1970s' depression coincided with increasing SO_2 emissions (Figure 3c). Air pollution not only directly harmed needle growth but may also have prompted lag effects via soil acidification. Moreover, it is probable that tree nutrition became imbalanced with disproportionate N uptake compared to base cations by elevated N deposition (Schulze 1989). The success of recent pollution mitigation initiatives is indicated by a rapid surge in Central European growth after ~1982, with the effects of forest management, climate warming, and atmospheric fertilization potentially also amplifying this boost. In contrast, Mediterranean forest ecosystems suffer from a long-term drying trend since the 1970s (Figure 3b). Fir growth in the Spanish Pyrenees likely showed local drought-induced post-1980s decline (Figure 3a), and affected stands were not able to increase their water-use efficiency (Camarero *et al.* 2011; Linares and Camarero 2012), despite rising atmospheric CO_2 concentrations.

It is possible that there has been some underestimation of the 1970s Central European forest dieback and overestimation of the subsequent growth release as a result of tree-ring sampling bias, given that the 20th century is represented by surviving trees only, which have recently grown under lower and wider canopy structures in more open habitats. Estimates of early industrial pollution and the resulting atmospheric composition are also not sufficiently resolved in space and time to accurately explain any direct vegetation responses; likewise, the historical development of acidification in different soil types is not well understood. The relative importance of forest insect and disease outbreaks to observed growth declines observed here remains unclear due to the lack of consistent regional outbreak records. The possibility that insect pests or fungal pathogens functioned as either primary or secondary factors contributing to the mid-1970s fir decline still represents an unanswered question (Houston 1987), particularly considering that these agents may have interacted with the extreme drought that occurred in 1976 (Spiecker 1995).

This study suggests that silver fir growth, in contrast with the growth of other tree species, will benefit from a projected warmer but not drier climate in mesic areas, whereas more southern habitats near the species' Mediterranean distribution limit are already exhibiting drought-induced growth depression, which will become even more critical in a drier future. These spatially diverse trends, projected to continue under climate change, could potentially be important to recent large-scale estimates of terrestrial carbon budgets, and thus should be considered for inclusion in certain ecological and biogeochemical models.

Acknowledgements

We thank ZAMG and CRU for making instrumental data available, P Collins for processing pollen data, and all ITRDB contributors and the KNMI climate explorer team. UB was also supported by the Operational Programme of Education for Competitiveness of Ministry of Education, Youth and Sports of the Czech Republic (Project No CZ.1.07/2.3.00/20.0248).

References

Auer I, Böhm R, Jurkovic A, *et al.* 2007. HISTALP – historical instrumental climatological surface time series of the greater Alpine region 1760–2003. *Int J Climatol* **27**: 17–46.

Brázdil R, Pfister C, Wanner H, *et al.* 2005. Historical climatology in Europe – the state of the art. *Climatic Change* **70**: 363–430.

Büntgen U, Brazdil R, Heussner K-U, *et al.* 2011a. Combined dendro-documentary evidence of Central European hydroclimatic springtime extremes over the last millennium. *Quat Sci Rev* **30**: 3947–59.

Büntgen U, Tegel W, Nicolussi K, *et al.* 2011b. 2500 years of European climate variability and human susceptibility. *Science* **331**: 578–82.

Büntgen U, Kaczka RJ, Trnka M, and Rigling A. 2012a. Ensemble estimates reveal a complex hydroclimatic sensitivity of pine growth at Carpathian cliff sites. *Agr Forest Meteorol* **160**: 100–09.

Büntgen U, Tegel W, Heussner K-U, *et al.* 2012b. Effects of sample size in dendroclimatology. *Clim Res* **53**: 263–69.

Büntgen U, Kyncl T, Ginzler C, *et al.* 2013. Filling the Eastern European gap in millennium-long temperature reconstructions. *P Natl Acad Sci USA* **110**: 1773–78.

Bürgi M and Schuler A. 2003. Driving forces of forest management – an analysis of regeneration practices in the forests of the Swiss Central Plateau during the 19th and 20th century. *Forest Ecol Manag* **176**: 173–83.

Camarero JJ, Bigler C, Linares JC, and Gil-Pelegrin E. 2011. Synergistic effects of past historical logging and drought on the decline of Pyrenean silver fir forests. *Forest Ecol Manag* **262**: 759–69.

Collins PM, Davis BAS, and Kaplan JO. 2012. The mid-Holocene vegetation of the Mediterranean region and southern Europe, and comparison with the present day. *J Biogeogr* **39**: 1848–61.

Colombaroli D, Marchetto A, and Tinner W. 2007. Long-term interactions between Mediterranean climate, vegetation and fire regime at Lago di Massaciuccoli (Tuscany, Italy). *J Ecol* **95**: 755–70.

Dobrovolný P, Moberg A, Brazdil R, *et al.* 2010. Monthly, seasonal and annual temperature reconstructions for Central Europe derived from documentary evidence and instrumental records since AD 1500. *Climatic Change* **101**: 96–107.

Feurdean A and Willis KJ. 2008. Long-term variability of *Abies alba* in NW Romania: implications for its conservation management. *Divers Distrib* **14**: 1004–17.

Fyfe RM, de Beaulieu JL, Binney H, *et al.* 2009. The European Pollen Database: past efforts and current activities. *Veg Hist Archaeobot* **18**: 417–24.

Houston DR. 1987. Forest tree declines of past and present: current understanding. *Can J Plant Pathol* **9**: 4349–60.

Innes JL. 1987. Air pollution and forestry. Forestry Commission Bulletin number 70. London, UK: HMSO.

Kandler O and Innes JL. 1995. Air pollution and forest decline in Central Europe. *Environ Pollut* **90**: 171–80.

Körner C. 2006. Plant CO_2 responses: an issue of definition, time and resource supply. *New Phytol* **172**: 393–411.

Linares JC and Camarero JJ. 2012. From pattern to process: linking intrinsic water-use efficiency to drought-induced forest decline. *Glob Change Biol* **18**: 1000–15.

Schulze ED. 1989. Air pollution and forest decline in a spruce (*Picea abies*) forest. *Science* **244**: 776–83.

Schütt P and Cowling EB. 1985. Waldsterben, a general decline of forests in Central Europe: symptoms, development, and possible causes. *Plant Dis* **69**: 548–58.

Spiecker H. 1995. Growth dynamics in a changing environment – long-term observations. *Plant Soil* **168**: 555–61.

Thomas RQ, Canham CD, Weathers KC, and Goodale CL. 2008. Increased tree carbon storage in response to nitrogen deposition in the US. *Nat Geosci* **3**: 13–17.

Tinner W and Lotter AF. 2006. Central European vegetation response to abrupt climate change at 8.2 ka. *Geology* **29**: 551–54.

van Aardenne J, Dentener F, Olivier J, *et al.* 2001. A 1° × 1° resolution data set of historical anthropogenic trace gas emissions for the period 1890–1990. *Global Biogeochem Cy* **15**: 909–28.

van Breemen N, Burrough PA, Velthorst EV, *et al.* 1982. Soil acidification from atmospheric ammonium sulphate in forest canopy throughfall. *Nature* **299**: 548–50.

Author contributions

UB and WTegel designed the study and analyzed the data with input from all authors. UB, WTegel, K-UH, JH, RK, TK, JK, JJC, and MC sampled and compiled tree-ring measurements. JOK and RB provided pollen and documentary data, respectively. UB, AL, and WTegel wrote the article with input from all authors.

[5]*Environmental Engineering Institute, Ecole Polytechnique Fédérale de Lausanne, Lausanne, Switzerland;* [6]*Institute of Geography, Masaryk University, Brno, Czech Republic;* [7]*Helmholtz Centre Potsdam, GFZ German Research Centre for Geosciences, Potsdam, Germany;* [8]*University of Padova, Dip TeSAF, Legnaro, Italy;* [9]*German Archaeological Institute DAI, Berlin, Germany;* [10]*Jahrringlabor Hofmann, Nürtingen, Germany;* [11]*Labor Dendron, Basel, Switzerland;* [12]*Moravian Dendro-Labor, Brno, Czech Republic;* [13]*ARAID-Instituto Pirenaico de Ecología IPE-CSIC, Zaragoza, Spain;* [14]*Department of Ecology, University of Barcelona, Barcelona, Spain;* [15]*Institute of Plant Sciences, University of Bern, Bern, Switzerland;* [16]*Department of Geography, Johannes Gutenberg University, Mainz, Germany;* [17]*Northern Research Station, USDA Forest Service, Morgantown, WV*

WebFigure 1. *(a) Visual examples of living and historical silver fir (*Abies alba*) sampling sites, including (from left to right) a forest stand, a high-resolution micro-section of one annual ring (40× amplified), a historical farm house, a late-medieval chapel, a roof construction, and a mining construction. (b) European fir distribution and the three core sampling regions (West, Mid, East); reproduced from Büntgen* et al. *(2011a).*

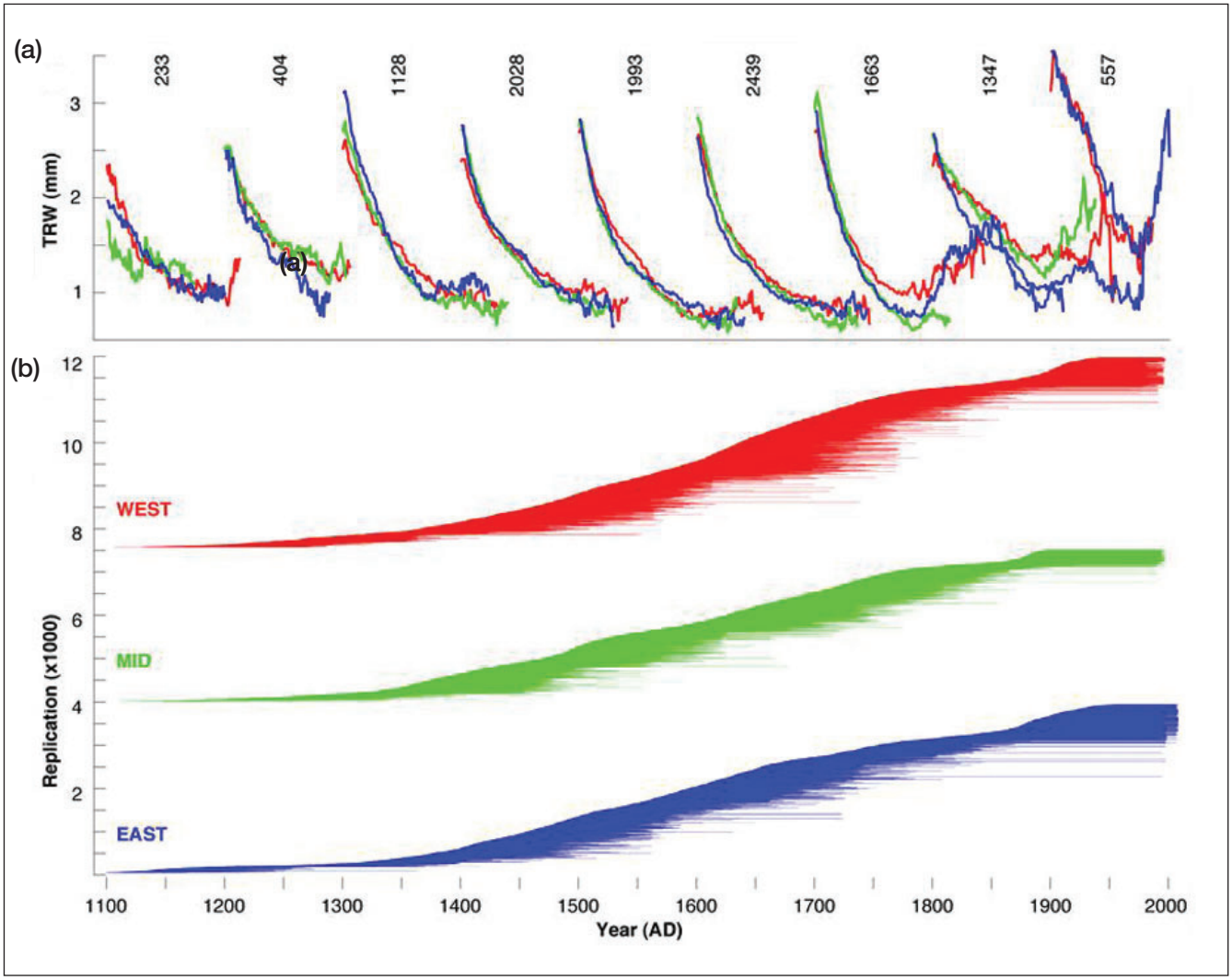

WebFigure 2. *(a) Regional curves (RCs) of the three core subsets (West, Mid, East) of silver fir growth truncated at 20 series and separately calculated for each century (see also Büntgen* et al. *[2012] for details), with the vertical numbers indicating sample size per century. (b) Temporal distribution of individual measurement series (TRW = tree-ring width). All RCs were calculated from age-aligned raw measurement series (Esper* et al. *2003), which were used to describe increment changes (y axis) in relation to cambial ages (x axis).*

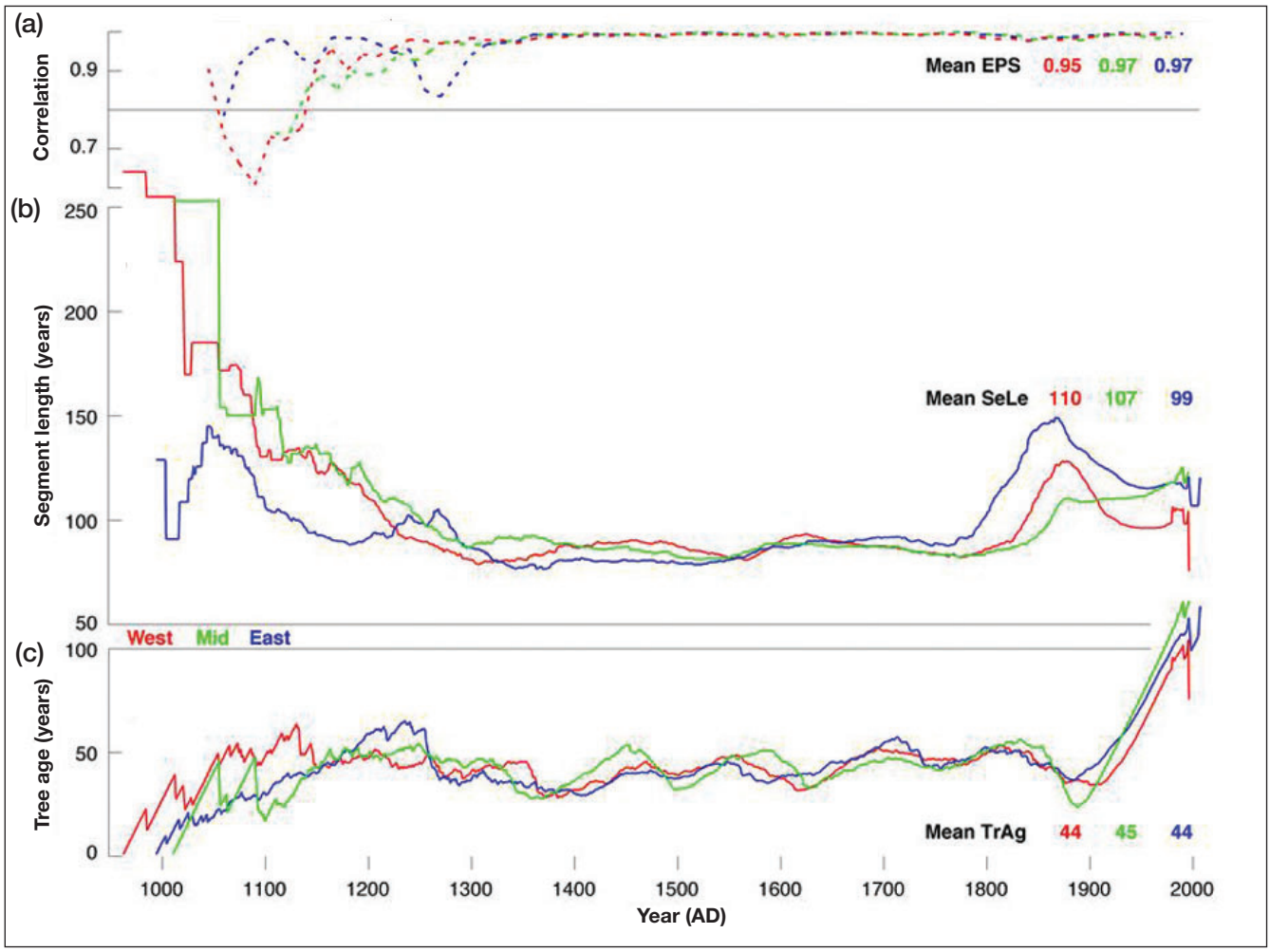

WebFigure 3. *(a) Expressed population signal (EPS; Wigley* et al. *1984) of the 11 873 individual silver fir ring-width measurement series shown per core region (West, Mid, East) and computed over 30-year windows lagged by 15 years. (b) Mean series length (SeLe) and (c) mean tree age (TrAg) of the three core region subsets (West, Mid, East) suggest most reliable chronology characteristics between ~1100 CE and 1900.*

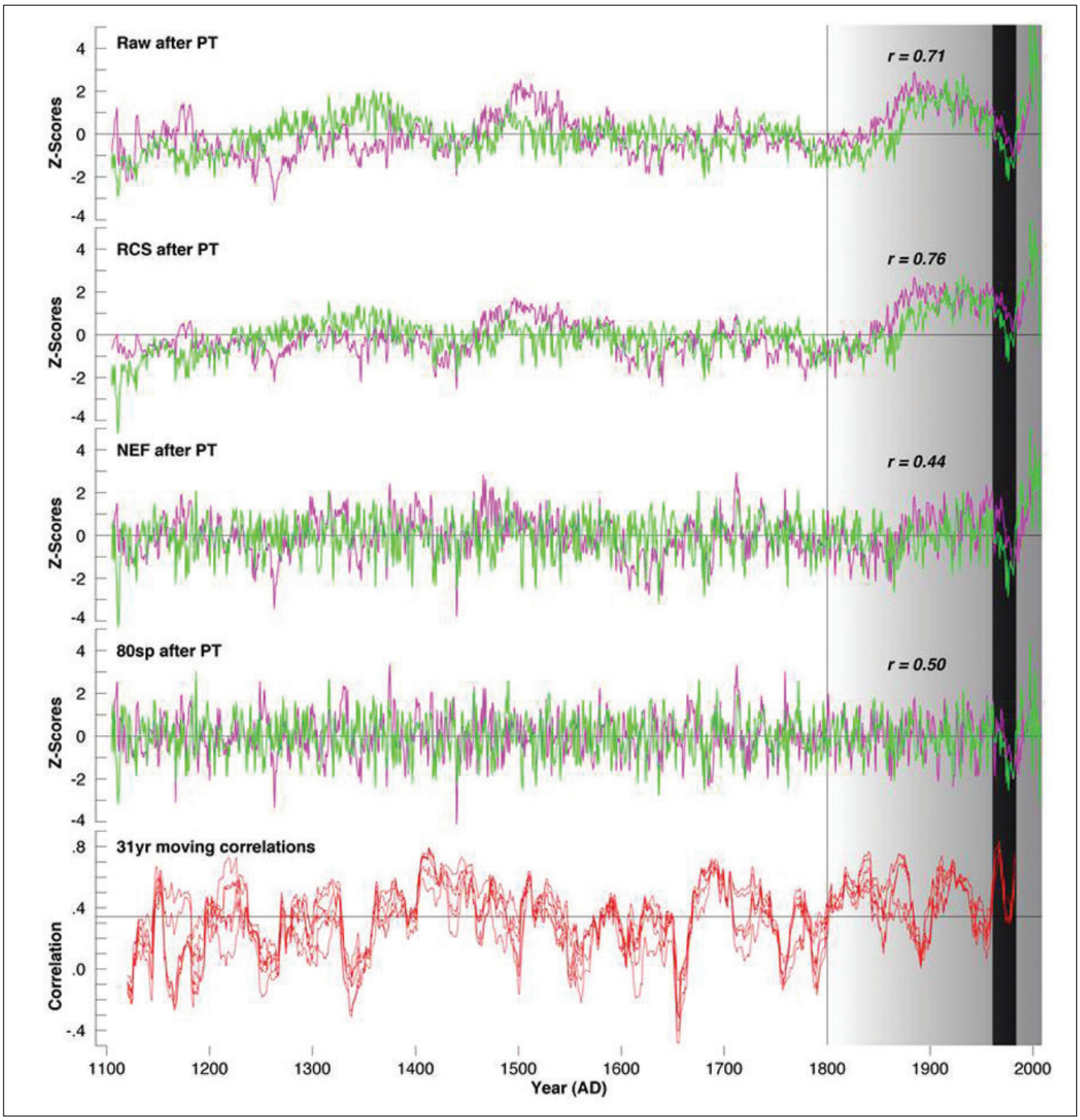

WebFigure 4. *Different silver fir chronologies (CORE; green) based on data that were averaged over the three core regions (West, Mid, East) are compared with the chronology from northern and central Italy (SA1; pink). Correlation coefficients refer to the well-replicated 1800–1998 common period, and moving correlations (red) are computed over 31-year intervals (at the bottom of the figure). Abbreviations of the different detrending methods: PT, power-transformation; NEF, negative exponential function; RCS, regional curve standardization; 80sp, 80-year long spline. Slightly different standardization techniques (ie detrending procedures) were applied to remove non-climatic, biological growth trends (so-called age-trends) from the raw ring-width measurement series and to test for possible influences of age-trend removal on high- to low-frequency preservation in the resulting chronologies (Büntgen* et al. *2013). In fact, cubic smoothing splines (SP) with 50% frequency-response cut-off at 20 and 80 years, as well as NEF, preserved inter-annual to decadal variability in the subsequent time series. The RCS allowed longer term trends to be captured (Esper* et al. *2003; Büntgen* et al. *2011b, 2012, 2013). Moreover, two different strategies of index calculation were considered to account for possible end-effect biases inherent in the chronology development process; ratios and residuals after PT were individually calculated between the original measurements and their corresponding curve fits (Cook and Peters 1997). We calculated mean chronologies using bi-weight robust means (Cook and Kairiukstis 1990), and temporal variance changes due to fluctuating sample size and inter-series correlation were stabilized (Osborn* et al. *1997).*

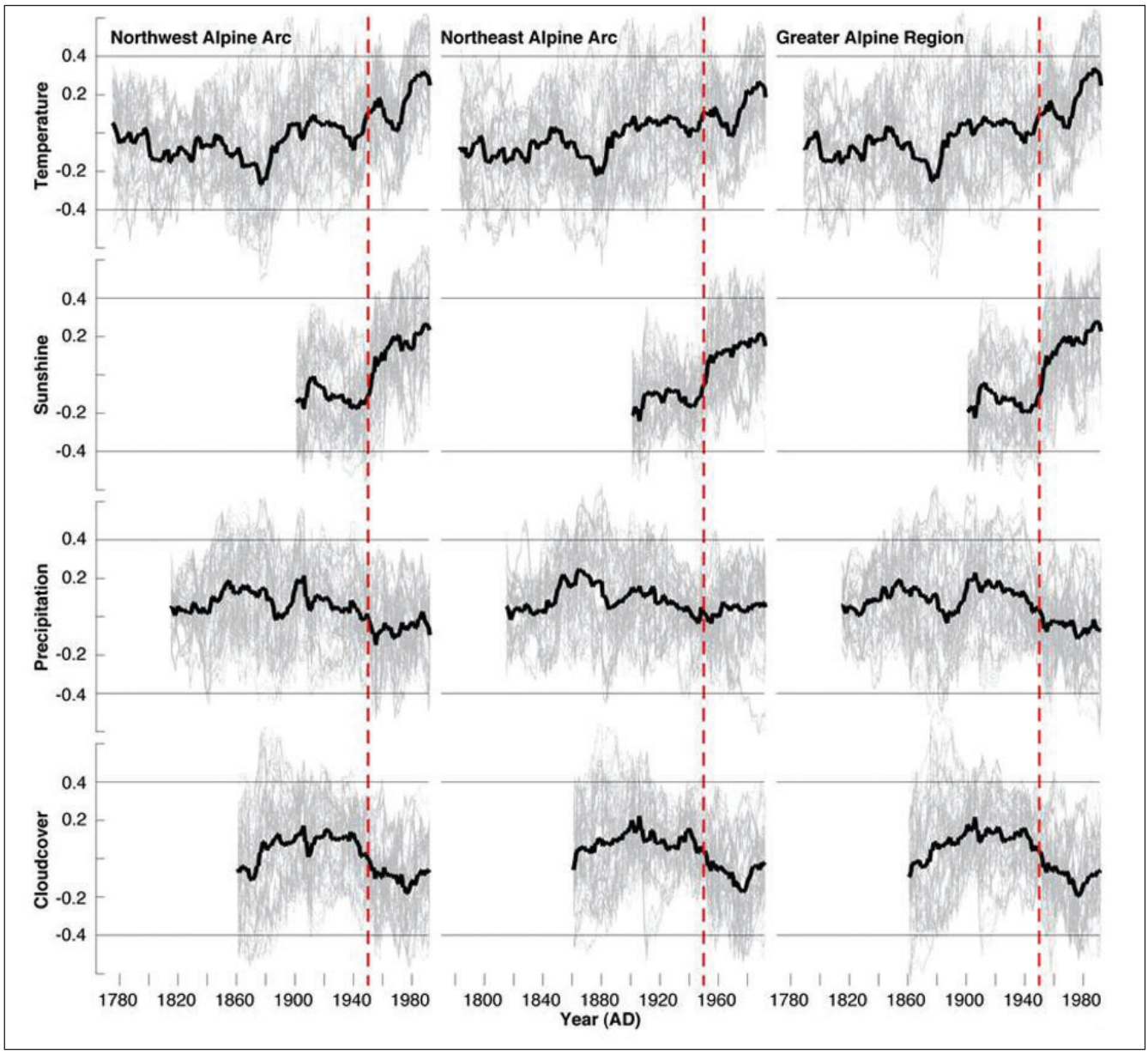

WebFigure 5. *A total of 1368 time-series of moving 31-year correlation coefficients that describe temporal changes (ie stability or instability) in the association between six slightly different silver fir chronologies and 19 monthly and seasonal resolved climatic targets, which were calculated for three geographical regions: Northwest Alpine Arc, Northeast Alpine Arc, and the Greater Alpine Region (Auer* et al. *2007). The six fir chronologies – based on raw measurements, raw measurements after power-transformation, RCS detrending, RCS detrending after power-transformation, negative exponential functions, and 80-year spline functions – were calculated from all ring-width measurement series of the three core regions (West, Mid, East). The monthly temperature, precipitation, sunshine, and cloudcover indices range from January–December, whereas the seven climatologically defined seasonal means include March–May, June–August, September–November, December–February, April–September, October–March, and annual. The red vertical lines are visually identified marks of possible response shifts.*

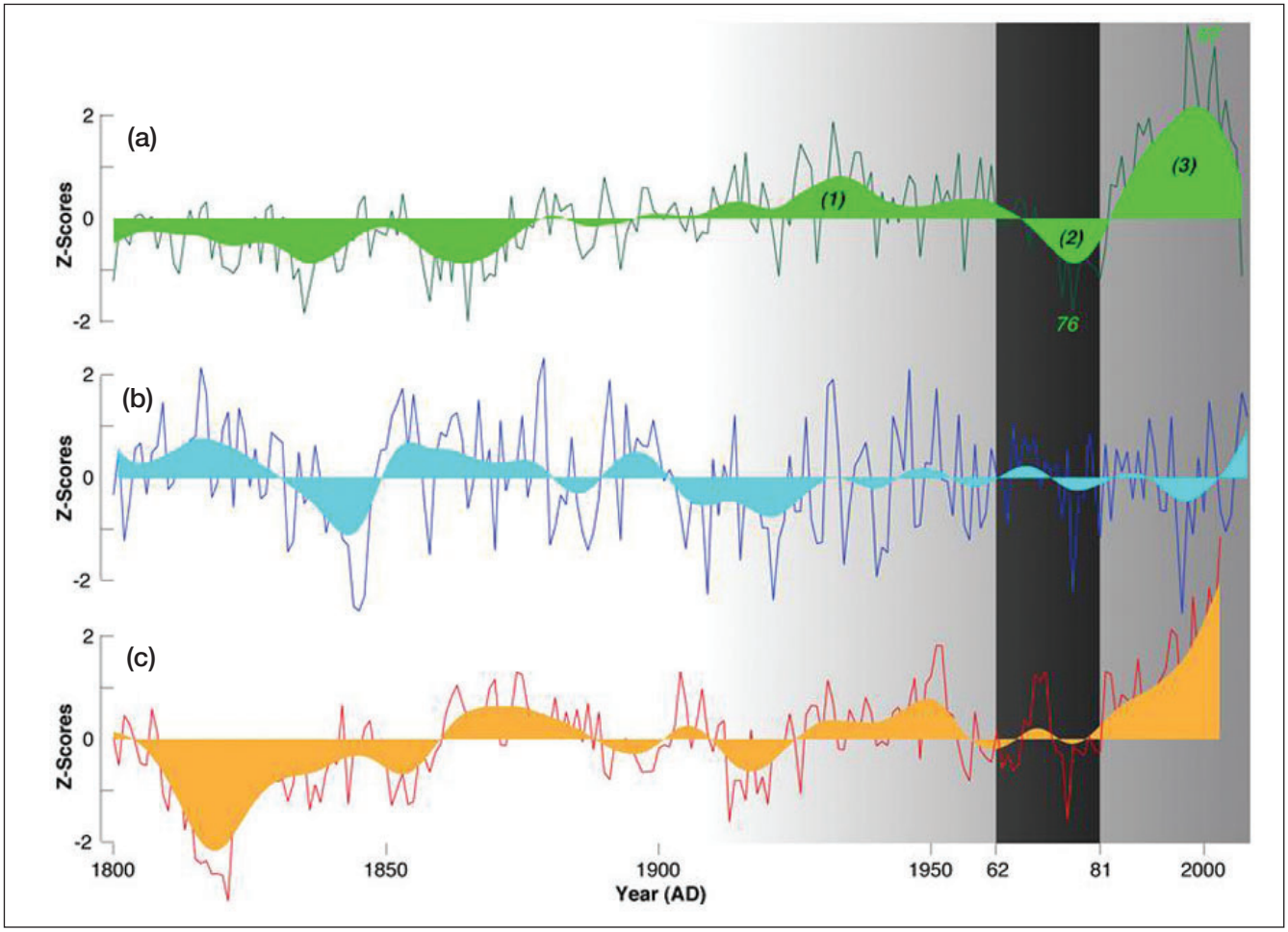

WebFigure 6. *Comparison of (a) silver fir growth averaged over the three Central European core regions (West, Mid, East) with (b) an oak-based reconstruction of Central European springtime precipitation variability and (c) a conifer-based reconstruction of Alpine-wide summer temperature variability, as introduced by* Büntgen et al. *(2011b). Thin curves refer to annual values, whereas the shadings derive from 20-year low-pass filtering. Superimposed on the silver fir chronology (a) are three phases of distinct growth changes and levels (1 = increase, 2 = decrease, 3 = release). The dark vertical bar denotes the prominent growth depression in Central European fir growth that roughly occurred between 1962 and 1981.*

WebTable 1. Dendrochronological characteristics and most relevant metadata of the seven different fir sampling subsets, including the number of series, the period covered, the average growth rate (AGR) in millimeters, the mean segment length (MSL) in years, and the first-order autocorrelation in r (Lag-1), as well as the study country and data source

Subset	*Series*	*Period*	*AGR*	*MSL*	*Lag-1*	*Country*	*Source*
West	4413	962–1996	1.84	81	0.79	France, Switzerland, Germany	Kontic, Tegel, ITRDB
Mid	3517	1010–1996	1.74	82	0.78	Germany	Hofmann, Heussner, ITRDB
East	3943	994–2007	1.76	85	0.76	Germany, Czech Republic	Kyncl, Heussner, ITRDB
EA1	773	1743–2011	2.45	88	0.79	Slovakia, Poland, Ukraine	Kyncl
SA1	500	1105–1998	1.82	136	0.83	Italy > 40°N	Career, ITRDB
SA2	249	1697–1999	2.06	148	0.82	Italy < 40°N	Career, Martinelli, Motta, Nola, ITRDB
SA3	741	1667–2000	2.45	96	0.80	Spain, France (Pyrenees)	Camarero, ITRDB

WebTable 2. Comparison of positive (+) and negative (–) Central European (core region) silver fir growth extremes (+ and –) with temperature and precipitation (T and P) indices based on documentary and instrumental evidence from the Czech Lands (CZ), Germany (D), and Switzerland (CH)

Year	*Region*	*Spring T/P indices*	*Summer T/P indices*	*Mar–Jun T/P indices*	*May T/P indices*
1503	-all	CH -/-, D -1/-3, CZ (0)/-	CH 1/-, D 8/-3, CZ 4/-6	CH -/-, D 1/-5, CZ (1)/-	CH -/-, D 1/-2, CZ 1/-3
1504	-all	CH -/-, D 2/-4, CZ 1/(-4)	CH 6/-, D 5/-4, CZ 5/(-3)	CH -/-, D 4/-6, CZ 3/(-5)	CH -/-, D 1/-2, CZ -/-2
1517	-WM	CH (-2)/(0), D 1/-6, CZ -/-	CH -/-, D 1/3, CZ -/-	CH -/-, D 2/-8, CZ -/-	CH -/-, D 1/-1, CZ -/-
1525	-ME	CH -/-, D -1/-2, CZ -/-	CH 0/(0), D 1/0, CZ 4/-	CH -/-, D -1/-2, CZ -/-	CH -/-, D -1/0, CZ -/-
1541	-all	CH -1/(1), D -1/-2, CZ -/-	CH 0/(1), D -1/0, CZ -/-	CH -2/(1), D 0/-4, CZ -/-	CH -1/1, D 0/-2, CZ -/-
1545	+ME	CH 0/2, D 1/0, CZ 0/-	CH 6/-2, D 4/-4, CZ 5/-	CH 2/3, D 1/-2, CZ 1/-	CH 0/1, D 0/-1, CZ 0/-
1558	+ME	CH 2/-2, D 3/0, CZ -/-	CH 1/-2, D 3/-2, CZ -/(-2)	CH 1/0, D 4/1, CZ -/-	CH 0/0, D 0/2, CZ 0/-
1563	+ME	CH 0/-1, D -3/-2, CZ -/(-1)	CH 1/2, D -5/5, CZ -4/5	CH 1/-1, D -5/0, CZ -/(0)	CH 1/0, D 0/-1, CZ -/-
1570	+WM	CH -7/1, D 0/4, CZ (-2)/-	CH -5/7, D -1/-1, CZ -/2	CH -7/3, D1/2, CZ -/-	CH -1/0, D 0/2, CZ -1/-
1590	-ME	CH -2/-5, D -2/-4, CZ (-1)/-	CH 5/-5, D 8/-7, CZ 8/-	CH -1/-6, D 1/-7, CZ (1)/-	CH -1/0, D -1/0, CZ -/0
1608	-ME	CH -1/-2, D -1/2, CZ -3/0	CH -7/5, D -5/-1, CZ -1/-	CH -3/0, D -3/3, CZ -4/-	CH 0/0, D 0/3, CZ 0/-
1616	-all	CH 0/-3, D 2/-3, CZ 2/-	CH 8/-7, D 6/-7, CZ 7/(-3 only one month)	CH 3/-6, D 5/-5, CZ 5/-	CH 0/-1, D 0/-1, CZ 0/-1
1624	-WM	CH 2/-2, D 2/0, CZ (-3)/(-2)	CH 1/2, D 5/0, CZ 3/-	CH 2/0, D 3/0, CZ (-1)/-	CH 1/-1, D 2/-1, CZ -/-1
1636	-all	CH 7/-7, D -1/-7, CZ -/-	CH 0/-1, D 1/2, CZ -/(-1)	CH 7/-8, D 1/-8, CZ -/-	CH 3/-3, D 1/-3, CZ -/-3
1641	+all	CH -3/1, D -1/1, CZ -3/-1	CH -2/(4), D -1/1, CZ -3/5	CH -5/3, D -1/1, CZ -3/0	CH -1/0, D 1/0, CZ -1/-2
1653	-all	CH 3/-4, D 1/-3, CZ -/-	CH 3/(-1), D -2/-5, CZ -/-	CH 6/-7, D 0/-5, CZ -/-	CH 3/-2, D 2/-2, CZ -/-2
1675	+all	CH -2/0, D -3/1, CZ -/-	CH -7/2, D -2/6, CZ -/-	CH -5/1, D -4/4, CZ -/-	CH -1/1, D -1/0, CZ -/-
1681	-all	CH -1/-1, D -2/-4, CZ (-1)/-	CH 3/-3, D 0/-4, CZ 0/-	CH -2/-1, D -2/-5, CZ (-3)/-	CH 1/0, D -2/0, CZ 1/0
1685	-WM	CH 2/-4, D -3/-2, CZ -/-	CH -6/3, D -4/5, CZ -4/-	CH -1/-2, D -5/-1, CZ -/-	CH 2/-2, D -1/-1, CZ -/-
1693	+WM	CH -6/8, D -3/4, CZ (-3)/(4)	CH 1/1, D 0/2, CZ 4/(-2)	CH -5/8, D -1/5, CZ (-1)/0	CH -2/3, D -2/2, CZ -2/2
1697	-all	CH -2/0, D -1/-2, CZ -1/-2	CH 0/1, D -1/1, CZ -4/2	CH -2/-1, D -1/-4, CZ -2/-3	CH 0/0, D 0/-1, CZ 0/0
1709	-ME	CH 0/3, D -1/3, CZ (-2)/-	CH -2/1, D -1/1, CZ -/-	CH -1/5, D -1/4, CZ -/-	CH -3/1, D -1/0, CZ -1/-
1713	+ME	CH -5/-2, D -5/2, CZ 0/1	CH -5/7, D -3/4, CZ 0/2	CH -7/0, D -6/2, CZ 0/1	CH -2/-2, D -2/1, CZ -1/0
1714	+WE	CH -7/-2, D -4/4, CZ -3/-	CH -1/0, D -3/1, CZ -/(3)	CH -7/-2, D -6/3, CZ (-3)/-	CH -2/-1, D -1/0, CZ -1/-
1720	-all	CH -2/3, D -4/2, CZ -3/-	CH -2/8, D -4/1, CZ -2/0	CH -3/6, D -7/1, CZ -4/-	CH 1/1, D 0/2, CZ -1/-
1724	+all	CH 1/2, D -3/3, CZ 0/0	CH 7/-5, D 2/-5, CZ 5/-5	CH 4/0, D -2/2, CZ 2/-2	CH 2/0, D 0/0, CZ 0/0
1759	+WM	CH -1/-2, D 1/-4, CZ -1/-3	CH 1/1, D 1/0, CZ 1/0	CH -1/-2, D 1/-3, CZ -1/-3	CH 0/-2, D 0/-3, CZ -2/0
1762	-all	CH 0/-4, D 2/-1, CZ 0/-3	CH 3/2, D -2/-1, CZ 1/-	CH 0/-3, D 2/-3, CZ 0/(-3)	CH 1/-2, D 2/1, CZ -1/-1
1772	+ME	CH -1/4, D -3/0, CZ 0/2	CH 3/0, D 0/-2, CZ -1/-3	CH 1/2, D -2/0, CZ -2/3	CH -1/2, D -3/-1, CZ 2/-1
1784	-WM	CH -1/1, D -1/-5, CZ -4/-1	CH 0/-1, D 3/-1, CZ 0/1	CH -1/0, D 1/-5, CZ -4/0	CH 2/-1, D 3/-3, CZ 0/-3
1787	+WM	CH -1/-2, D 2/0, CZ -2/2	CH 1/1, D 6/-4, CZ 0/-5	CH -1/-2, D 5/-2, CZ -2/0	CH -2/-3, D -1/-1, CZ -2/0
1796	+all	CH -3/-5, D -2/-5, CZ -4/-2	CH 0/0, D 3/2, CZ -2/2	CH -3/-4, D -2/-5, CZ -5/-1	CH 0/0, D 0/1, CZ -1/2
1812	-all	CH -4/-1, D -2/-1, CZ (-2)/-	CH -3/0, D -2/-4, CZ -2/6	CH -5/-1, D -2/-3, CZ -/-	CH 0/0, D 1/-1, CZ 0/-
1817	+WM	CH -5/-1, D -4/-1, CZ -4/5	CH -2/-1, D 0/-1, CZ 0/3	CH -5/-2, D -1/-2, CZ -3/7	CH -1/2, D -1/0, CZ -1/2
1829	+ME	CH 0/2, D -1/0, CZ -5/3	CH -2/0, D -3/3, CZ 1/4	CH -1/3, D -2/0, CZ -5/4	CH 0/-1, D 0/-1, CZ -2/-1
1835	-all	CH -1/-1, D -1/4, CZ -2/1	CH 1/-5, D 2/-3, CZ 2/-5	CH -1/-4, D -1/1, CZ 0/-1	CH 0/2, D 0/1, CZ 0/0
1846	+ME	CH 0/3, D 1/4, CZ 0/4	CH 5/0, D 9/-4, CZ 5/-3	CH 3/3, D 4/1, CZ 2/2	CH 0/0, D 0/0, CZ -1/2
1858	-WM	CH -2/0, D -4/-1	CH 2/-1, D 1/-3	CH 1/-3, D -1/-4	CH -2/1, D -2/0
1861	+WE	CH -2/-4, D -2/-2	CH 3/1, D 6/-2	CH -1/-3, D 1/-2	CH -1/-3, D -1/-1
1863	+WM	CH 1/-1, D 0/-2	CH 2/-1, D 2/0	CH 1/1, D 0/-1	CH 0/-1, D 0/-1
1865	-all	CH 3/-4, D 3/-3	CH 1/-2, D 2/-2	CH 3/-7, D 2/-5	CH 3/-1, D 3/0
1890	+all	CH 0/-1, D 0/0	CH -2/3, D -6/1	CH -1/-1, D -3/-1	CH 0/0, D 1/1
1893	-WM	CH 3/-5, D 4/-6	CH 1/-4, D 1/-3	CH 3/-6, D 4/-7	CH 0/-1, D 0/-2
1898	+WM	CH -2/0, D -1/2	CH -1/-1, D -2/-2	CH -3/0, D -2/2	CH -1/1, D -1/2
1916	+all	CH 0/-1, D 0/0	CH -4/4, D -5/0	CH -3/2, D -3/0	CH 0/-1, D 0/0
1922	-all	CH -1/3, D -1/2	CH -2/1, D -4/1	CH -1/4, D -1/2	CH 1/-1, D 2/-2
1929	-all	CH -2/-3, D -3/-3	CH 0/0, D 0/0	CH -2/-3, D -3/3	CH 0/-1, D 0/0
1940	-ME	CH 0/1, D 1/2	CH -2/1, D -4/3	CH 0/1, D 2/2	CH 0/1, D 0/0
1956	-all	CH -1/1, D -3/0	CH -4/3, D -6/3	CH -3/0, D -6/0	CH 0/0, D 0/0
1959	+ME	CH 3/-1, D 5/0	CH 2/-1, D 3/-3	CH 3/0, D 5/-1	CH 0/-1, D 0/0
1974	-WE	CH 2/-2, D 2/-2	CH 0/-1, D -5/0	CH 1/-2, D -1/-2	CH 0/0, D -1/0
1976	-all	CH 1/-3, D 0/-2	CH 5/-3, D 5/-5	CH 4/-6, D 3/-5	CH 1/0, D 1/-1

Notes: Silver fir growth extremes either occurred at the regional (WM = West–Mid, WE = West–East, ME = Mid–East) or subcontinental (all) scales. Indices in the table are calculated as sums of monthly indices in the given interval (eg from March, April, and May for spring). Indices in parentheses reflect incomplete documentary evidence when one month is missing. Source of T and P indices: CZ – Czech historical-climatological database, indices only up to 1854; D – www.hisklid.de; CH – Pfister (1999), Dobrovolný *et al.* (2010).

WebTable 3. Summary information of the 356 pollen profiles, with EPD referring to the "European Pollen Database"

Site name	*Longitude*	*Latitude*	*Elevation*	*Source*
Kamenicky	15.96	49.73	624	EPD
Aegelsee	7.54	46.64	989	EPD
Amsoldingersee	7.57	46.72	641	EPD
Amsoldingersee	7.57	46.72	641	EPD
Amsoldingersee	7.57	46.72	641	EPD
Altenweiher	6.99	48.01	926	EPD
Bois de Buchelbush	5.82	49.71	375	EPD
Bois de Buchelbush	5.82	49.71	375	EPD
Bois de Buchelbush	5.82	49.71	375	EPD
Buzenol	5.6	49.62	265	EPD
Bedlno	20.28	51.2	227	EPD
Ethe source du Cron	5.59	49.6	245	EPD
Tontelange Heideknapp	5.82	49.71	325	EPD
Bellefontaine	6.09	46.57	1093	EPD
Bois des Amerois	5.12	49.74	415	EPD
Abbaye d'Orval	5.34	49.64	215	EPD
Abbaye d'Orval	5.34	49.64	215	EPD
Abbaye d'Orval	5.34	49.64	215	EPD
Abbaye d'Orval	5.34	49.64	215	EPD
Abbaye d'Orval	5.34	49.64	215	EPD
Abbaye d'Orval	5.34	49.64	215	EPD
Abbaye d'Orval	5.34	49.64	215	EPD
Abbaye d'Orval	5.34	49.64	215	EPD
Blato	15.19	49.04	645	EPD
Blato	15.19	49.04	645	EPD
Boehnigsee Goldmoos	7.84	46.25	2061	EPD
Burgmoos	7.67	47.17	465	EPD
Burgmoos	7.67	47.17	465	EPD
Burgmoos	7.67	47.17	465	EPD
Burgmoos	7.67	47.17	465	EPD
Burgmoos	7.67	47.17	465	EPD
Burgmoos	7.67	47.17	465	EPD
Burgmoos	7.67	47.17	465	EPD
Burgmoos	7.67	47.17	465	EPD
Burgmoos	7.67	47.17	465	EPD
Cergowa Gora	21.7	49.53	495	EPD
Chranboz	15.36	49.75	480	EPD
Chranboz	15.36	49.75	480	EPD
Czajkow	21.28	50.78	206	EPD
Czajkow	21.28	50.78	206	EPD
Czajkow	21.28	50.78	206	EPD
Dürrenecksee-Moor	13.86	47.16	1700	EPD
Dvur Ansov	16.38	48.79	179	EPD
Fuchsschwanzmoos	13.9	47.11	1680	EPD
Giecz	17.36	52.31	100	EPD
Golkow	20.97	52.05	108	EPD
Hirschen Moor	8.09	47.83	962	EPD
Hroznotin	15.35	49.75	485	EPD
Imbramowice	16.58	50.89	175	EPD
Liptovsky Jan	19.67	49.04	660	EPD
Liptovsky Jan	19.67	49.04	660	EPD
Jasiel	21.88	49.37	680	EPD
Spoli	14.9	48.96	440	EPD
Velanská cesta	14.98	49.25	505	EPD
Cervene blato	14.93	48.85	470	EPD
Cervene blato	14.93	48.85	470	EPD

continued

WebTable 3. – *continued*

Site name	*Longitude*	*Latitude*	*Elevation*	*Source*
Cervene blato	14.93	48.85	470	EPD
Borkovicka blata	14.9	49.21	415	EPD
Borkovicka blata	14.9	49.21	415	EPD
Branna	14.93	48.95	450	EPD
Barbora	14.93	48.94	460	EPD
Svarcenberk	14.89	49.13	420	EPD
Jestrebske blato	14.59	50.6	259	EPD
Kletnia Stara	21.67	51.63	135	EPD
Komorany	13.5	50.5	231	EPD
Komorany	13.5	50.5	231	EPD
Komorany	13.5	50.5	231	EPD
Etang du Lautrey	5.86	46.58	788	EPD
Lobsigensee	7.29	47.03	514	EPD
Loucky	15.5	49.32	560	EPD
Beaufort Birkenbach	6.12	49.84	360	EPD
Berdorf Aesbaach	6.43	49.83	190	EPD
Breidfeld	6.06	50.12	440	EPD
Echternach	6.23	49.79	170	EPD
Echternach	6.23	49.79	170	EPD
Echternach	6.23	49.79	170	EPD
Pettange sur Alzette	6.1	49.78	218	EPD
Reisdorf	6.3	49.85	369	EPD
Reisdorf	6.3	49.85	369	EPD
Reisdorf	6.3	49.85	369	EPD
Reisdorf	6.3	49.85	369	EPD
Reisdorf	6.3	49.85	369	EPD
Reisdorf	6.3	49.85	369	EPD
Malcin	15.41	49.66	520	EPD
Mokre louky (South)	14.83	48.83	425	EPD
Mokre louky (North)	14.83	49.16	425	EPD
Moerbeke	4.94	51.17	4	EPD
Olbramovice	16.4	48.99	205	EPD
Ostrow	19.55	51.47	223	EPD
Palasiny	15.48	49.68	520	EPD
Palasiny	15.48	49.68	520	EPD
Podhorany	20.75	49	598	EPD
Puscizna Rekowianska	19.81	49.48	656	EPD
Rasna	15.37	49.23	680	EPD
Regetovka	21.27	49.42	515	EPD
Rezabinec	14.11	49.25	369	EPD
Rotsee	8.32	47.07	419	EPD
Rotsee	8.32	47.07	419	EPD
Rosle Nowe	18.91	52.13	110	EPD
Roztoki	21.58	49.71	230	EPD
Roztoki	21.58	49.71	230	EPD
Dürrenecksee-Moor	13.86	47.16	1700	EPD
Hozelec	18.3	49.05	685	EPD
Skrecon	18.38	49.88	203	EPD
Skrecon	18.38	49.88	203	EPD
Slopiec	20.78	50.78	248	EPD
Slopiec	20.78	50.78	248	EPD
Moselotte	7	48.03	1290	EPD
Spisska Bela	20.45	49.18	625	EPD
Suchedniow	20.85	51.05	255	EPD
Svatoborice-Mistrin	17.16	48.83	175	EPD
Szymbark	21.1	49.63	465	EPD
Tarnowiec	21.61	49.7	220	EPD

continued

WebTable 3. – *continued*

Site name	*Longitude*	*Latitude*	*Elevation*	*Source*
Lake Balaton (Southwest)	17.73	46.81	104	EPD
Lake Balaton (Center)	17.4	46.74	104	EPD
Lake Balaton (Northeast)	18.1	47	104	EPD
Trumer Moos	13.06	47.93	500	EPD
Grosses Überling Schattseit-Moor	13.9	47.16	1750	EPD
Vernerovice	16.25	50.1	450	EPD
Velke Nemcice	16.68	48.99	177	EPD
Vracov	17.2	48.97	192	EPD
Zavidkovice	15.4	49.64	430	EPD
Zbudovska blata	14.33	49.83	380	EPD
Zbudovska blata	14.33	49.83	380	EPD
Wasenmoos beim Zellhof	13.1	47.98	505	EPD
Zirbenwaldmoor	11.02	46.85	2150	EPD
Zirbenwaldmoor	11.02	46.85	2150	EPD
Zsombo Swamp	19.99	46.36	92	EPD
Zyrardow	20.44	52.05	117	EPD
Jaslo	21.46	49.78	250	EPD
Bleekemeer	5.75	52.25	25	EPD
Bosscherheide	6.09	51.57	18	EPD
Georgenfelder Hochmoor	13.75	50.75	860	EPD
Krumpa	11.85	51.3	71	EPD
Mariahout	5.54	51.52	14	EPD
Meerfelder Maar	6.75	50.1	336	EPD
Notsel	4.76	51.55	5	EPD
Schwemm	12.3	47.65	664	EPD
Schwemm	12.3	47.65	664	EPD
Schwemm	12.3	47.65	664	EPD
Schwemm	12.3	47.65	664	EPD
Holzmaar	8.87	50.11	425	EPD
Uddelermeer	5.76	52.23	26	EPD
Le Beillard	6.8	48.07	605	EPD
Bobrov	19.56	49.44	620	EPD
Velky Ded	17.21	50.08	1380	EPD
Zlatnicka Dolina	19.28	49.51	850	EPD
Les Enfers	7.16	47.25	960	EPD
Frasne	6.16	46.83	840	EPD
Jedlova	19.66	49.5	650	EPD
Velky Maj	17.21	50.05	1365	EPD
Moossalmmoor	13.51	47.75	740	EPD
Ödenseemoor	13.63	47.61	770	EPD
Rödschitzmoor	13.9	47.55	790	EPD
Tourbière les Veaux	7.09	47.24	1020	EPD
Gorno	20.83	50.85	240	EPD
La Beuffarde	6.42	46.82	1111	EPD
La Grande Pile	6.5	47.73	330	EPD
Holzmaar	8.87	50.11	425	EPD
Bosscherheide	6.09	51.57	18	EPD
Borkovicka blata	14.9	49.21	415	EPD
Rodenbourg Bretzboesh	6.27	49.69	285	EPD
Rotsee	8.32	47.07	419	EPD
Vracov	17.2	48.97	192	EPD
Schwemm	12.3	47.65	664	EPD
Aegelsee	7.54	46.64	989	EPD
Flaje Kiefern	13.53	50.7	760	EPD
Wolbrom	19.76	50.38	375	EPD
Jammertal	9.72	48.1	578	EPD

continued

WebTable 3. – *continued*

Site name	*Longitude*	*Latitude*	*Elevation*	*Source*
Breitnau-Neuhof	8.06	47.93	986	EPD
Durchenbergried	8.98	47.78	432	EPD
Feuenried	8.91	47.75	407	EPD
Hornstaad/Bodensee	9.01	47.7	385	EPD
Steerenmoos	8.2	47.8	1000	EPD
Wangen/Bodensee	8.93	47.66	395	EPD
Nussbaumer Seen	8.83	47.61	434	EPD
Nussbaumer Seen	8.83	47.61	434	EPD
Nussbaumer Seen	8.83	47.61	434	EPD
Grosser Treppelsee	14.45	52.15	52	EPD
Kozli	14.02	49.37	460	EPD
Älbi Flue	7.58	46.35	1850	EPD
Aletschwald	8.01	46.23	2017	EPD
Aletschwald	8.01	46.23	2017	EPD
Aletschwald	8.01	46.23	2017	EPD
Aletschwald	8.01	46.23	2017	EPD
Bachalpsee	8.01	46.4	2265	EPD
Baldeggersee	8.28	47.16	463	EPD
La Grande Basse	6.95	48.05	945	EPD
Alp Lüsga Belalp 1	7.59	46.23	2330	EPD
Alp Lüsga Belalp 2	7.58	46.23	2290	EPD
Bibersee	8.28	47.13	429	EPD
Bitsch-Naters	7.59	46.2	1030	EPD
Bodmen, Alp Bel	7.57	46.21	1970	EPD
Bodmen, Alp Bel	7.57	46.21	1970	EPD
Bodmen, Alp Bel	7.57	46.21	1970	EPD
Lac de Bretaye	7.04	46.19	1780	EPD
Untere Bunschleren, Boltigen	7.25	46.36	1680	EPD
Cinuskel	10.01	46.38	1615	EPD
Dossaccio, Bormio	10.2	46.28	1730	EPD
Dossaccio, Bormio	10.2	46.28	1730	EPD
Dossaccio, Bormio	10.2	46.28	1730	EPD
Dossaccio, Bormio	10.2	46.28	1730	EPD
Eggen ob Blatten	7.59	46.22	1645	EPD
Eggen ob Blatten	7.59	46.22	1645	EPD
Eggen ob Blatten	7.59	46.22	1645	EPD
Eggen ob Blatten	7.59	46.22	1645	EPD
Etang de la Gruère	7.04	47.23	1005	EPD
Etang de la Gruère	7.04	47.23	1005	EPD
Etang de la Gruère	7.04	47.23	1005	EPD
Feld Alp Holzmatten	8	46.39	2130	EPD
Gänsemoos, Schwarzenburg	7.21	46.5	795	EPD
Gamperfin	9.22	47.1	1320	EPD
Gerzensee	7.32	46.49	603	EPD
Gondo Alpjen	8.06	46.12	1635	EPD
Grächen See	7.5	46.11	1710	EPD
Grächen See	7.5	46.11	1710	EPD
Greicheralp, Riederalp	8.01	46.22	1910	EPD
Hagelseeli	8.02	46.4	2339	EPD
Grünsee, Reschenscheideck	10.28	46.51	1836	EPD
Hängstli	7.49	46.47	1260	EPD
Mittlere Hellelen	7.5	46.16	1520	EPD
Mittlere Hellelen	7.5	46.16	1520	EPD
Hinterburgseeli	8.04	46.43	1510	EPD
Il Fuorn	10.12	46.39	1805	EPD
Lac d'Aï	7	46.21	1891	EPD
Lai Nair, Schuls-Tarasp	10.31	46.78	1546	EPD

continued

WebTable 3. – *continued*

Site name	*Longitude*	*Latitude*	*Elevation*	*Source*
Leysin, Les Léchières	7.01	46.2	1255	EPD
Linden	7.41	46.51	900	EPD
Juf Plan	10.25	46.62	2225	EPD
Hopschensee	8.01	46.15	2017	EPD
Hopschensee	8.01	46.15	2017	EPD
Hopschensee	8.01	46.15	2017	EPD
Chutti, Boltigen	7.23	46.38	925	EPD
Chutti, Boltigen	7.23	46.38	925	EPD
Chutti, Boltigen	7.23	46.38	925	EPD
Etang de Luissel, Bex	7.01	46.14	540	EPD
Macun,Val Zeznina ob Zernez	10.04	46.42	2617	EPD
Mont Carré, Hérémence	7.22	46.09	2290	EPD
Lörmoos, Bern	7.24	46.59	583	EPD
Lörmoos, Bern	7.24	46.59	583	EPD
Lörmoos, Bern	7.24	46.59	583	EPD
Motta Naluns	10.26	46.81	2170	EPD
Oberaar	8.15	46.32	2315	EPD
Obergestelen, Zweisimmen	7.26	46.34	1810	EPD
Oppligen	7.35	46.49	560	EPD
Pillon, Gsteig-Diablerets	7.11	46.21	1670	EPD
Rotsee	8.32	47.07	419	EPD
Rotsee	8.32	47.07	419	EPD
Alpi di Robièi,Val Bavona	8.51	46.44	1892	EPD
Alpi di Robièi,Val Bavona	8.51	46.44	1892	EPD
Alpi di Robièi,Val Bavona	8.51	46.44	1892	EPD
Praz Rodet	6.17	46.56	1040	EPD
Palü Lunga ob Ramosch	10.37	46.84	1890	EPD
Seebergsee	7.46	46.61	1831	EPD
Trepalle, Livigno	10.18	46.51	2030	EPD
Rotmoos-Eriz	7.84	46.79	1190	EPD
Saanenmöser	7.31	46.51	1256	EPD
Sägistalsee	7.97	46.67	1935	EPD
Schönwies	11.02	46.84	2260	EPD
Schöpfenwaldmoor	7.5	46.44	1450	EPD
Schwarzsee FR	7.28	46.67	1046	EPD
Schwarzsee, Reschenscheideck	10.47	46.86	1721	EPD
Simplon/Gampisch-Alter Spittel	8.01	46.23	1885	EPD
Schwendital	8.98	47.07	1070	EPD
Süftenenegg	7.39	46.73	1555	EPD
Süftenenegg	7.39	46.73	1555	EPD
Süfternen-Grönegg	7.39	46.73	1520	EPD
Trogenmoos	7.86	46.76	1470	EPD
Umbrail	10.42	46.54	2490	EPD
Xirès, Montana	7.47	46.3	1445	EPD
Etang d'y Cor, Montana	7.47	46.31	1500	EPD
Wallbach, Lenk	7.4	46.42	1885	EPD
Wallbach, Lenk	7.4	46.42	1885	EPD
Wallbach, Lenk	7.4	46.42	1885	EPD
Wallbach, Lenk	7.4	46.42	1885	EPD
Wachseldorn Untermoos	7.73	46.82	980	EPD
Wachseldorn Untermoos	7.73	46.82	980	EPD
Wachseldorn Untermoos	7.73	46.82	980	EPD
Waxeckalm	11.5	47.02	1875	EPD
Dortmunder Hütte	11	47.1	1880	EPD
Mieminger See	10.97	47.29	800	EPD
Katzenloch	11.12	47.34	1220	EPD
Seefelder See	11.19	47.32	1200	EPD

continued

WebTable 3. – *continued*

Site name	*Longitude*	*Latitude*	*Elevation*	*Source*
Kirchbichl	12.09	47.51	512	EPD
Egelsee	12.17	47.61	549	EPD
Miesberg	12.27	47.64	670	EPD
Lutzenberg	12.36	47.46	815	EPD
Giering	12.35	47.47	820	EPD
Hasenmoos	12.37	47.47	770	EPD
Wasenmoos	12.41	47.3	1205	EPD
Wasenmoos	12.41	47.3	1205	EPD
Sommersüss	11.67	46.76	870	EPD
Rinderplatz	11.49	46.64	1780	EPD
Dura-Moor	11.45	46.64	2080	EPD
Malschötscher Hotter	11.45	46.66	2050	EPD
Schwarzsee	11.43	46.66	2033	EPD
Franz Senn-Hütte	11.88	47.35	2115	EPD
Grünau Moor	11.45	47.03	2190	EPD
Buntes Moor	11.3	47.06	2285	EPD
Moor Alpenrose	11.77	47.08	1880	EPD
Atemlöchermoos	11.01	46.93	1790	EPD
Pillermoos Untergurgl	11.04	46.9	1780	EPD
Wildmoos	11.01	46.95	1435	EPD
Krotenweiher	11.41	47.07	1310	EPD
Lanser Moor	11.42	47.24	840	EPD
Lanser Moor	11.42	47.24	840	EPD
Lanser Moor	11.42	47.24	840	EPD
Zotensenk	11.86	47.42	560	EPD
Zotensenk	11.86	47.42	560	EPD
Gerlos	12.13	47.24	1590	EPD
Moor am Rofenberg	10.82	46.82	2760	EPD
Le Loclat	6.99	47.02	432	EPD
Le Loclat	6.99	47.02	432	EPD
Le Loclat	6.99	47.02	432	EPD
Le Loclat	6.99	47.02	432	EPD
Le Loclat	6.99	47.02	432	EPD
Murifeld, Bern	7.28	46.56	554	EPD
Murifeld, Bern	7.28	46.56	554	EPD
Lac du Mont d'Orge, Sion	7.2	46.14	640	EPD
Lac du Mont d'Orge, Sion	7.2	46.14	640	EPD
Lac du Mont d'Orge, Sion	7.2	46.14	640	EPD
Lac du Mont d'Orge, Sion	7.2	46.14	640	EPD
Lac du Mont d'Orge, Sion	7.2	46.14	640	EPD
Alpi di Robièi,Val Bavona, Bodenprofil	8.51	46.44	1965	EPD
Meerfelder Maar	6.75	50.1	336	EPD
Fuschlsee	13.26	47.78	663	EPD
Bruckmisse	8.64	48.73	670	EPD
Bruckmisse	8.64	48.73	670	EPD
Bruckmisse	8.64	48.73	670	EPD
Glaswaldsee	8.24	48.42	839	EPD
Wildseemoor bei Kaltenbronn	8.45	48.71	909	EPD
Wildseemoor bei Kaltenbronn	8.45	48.71	909	EPD
Wilder See beim Ruhestein	8.23	48.56	910	EPD
Lac Superieur de Fully	7.09	46.17	2135	EPD
Ahlequellmoor	9.5	51.73	300	PANGAEA
Bruchberg-1	10.49	51.78	910	PANGAEA
Bruchberg-2	10.46	51.75	825	PANGAEA
Luederholz-1	10.3	51.68	228	PANGAEA
Luttersee-1	10.16	51.57	162	PANGAEA

continued

WebTable 3. – *continued*

Site name	*Longitude*	*Latitude*	*Elevation*	*Source*
Luttersee-2	10.16	51.57	164	PANGAEA
Meerfelder Maares	6.75	50.1	336	PANGAEA
Mochowsee	14.19	51.99	45	PANGAEA
Rappershausen1	10.39	50.37	383	PANGAEA
Silberhohl	10.18	51.91	180	PANGAEA
Sonnenberger Moor	10.51	51.76	780	PANGAEA
Weissenstadter Forst	11.88	50.13	725	PANGAEA
Csoszhalom	21.2	47.95	91	pers com
Feher-to	20.65	46.45	86	pers com
Nagymohos Holocene	20.45	48.38	294	pers com
Nagymohos Pleistocene	20.45	48.38	294	pers com
Sarlo-hat	21.16	47.96	86	pers com
Imola-CSG50-Csogle	17.23	47.23	100	pers com
Imola-PEB88-Poloske	16.93	46.75	150	pers com
Imola-ZV63	17.21	46.65	104	pers com
Noricka Graba	16.01	46.62	240	digitized

WebReferences

Auer I, Böhm R, Jurkovic A, *et al.* 2007. HISTALP – historical instrumental climatological surface time series of the greater Alpine region 1760–2003. *Int J Climatol* **27**: 17–46.

Büntgen U, Brazdil R, Heussner K-U, *et al.* 2011a. Combined dendro-documentary evidence of Central European hydroclimatic springtime extremes over the last millennium. *Quaternary Sci Rev* **30**: 3947–59.

Büntgen U, Tegel W, Nicolussi K, *et al.* 2011b. 2500 years of European climate variability and human susceptibility. *Science* **331**: 578–82.

Büntgen U, Tegel W, Heussner K-U, *et al.* 2012. Effects of sample size in dendroclimatology. *Clim Res* **53**: 263–69.

Büntgen U, Kyncl T, Ginzler C, *et al.* 2013. Filling the Eastern European gap in millennium-long temperature reconstructions. *P Natl Acad Sci USA* **110**: 1773–78.

Cook ER and Kairiukstis LA. 1990. Methods of dendrochronology: applications in environmental science. Dordrecht, the Netherlands: Kluwer.

Cook ER and Peters K. 1997. Calculating unbiased tree-ring indices for the study of climatic and environmental change. *Holocene* **7**: 361–70.

Dobrovolný P, Moberg A, Brazdil R, *et al.* 2010. Monthly, seasonal and annual temperature reconstructions for Central Europe derived from documentary evidence and instrumental records since AD 1500. *Climatic Change* **101**: 96–107.

Esper J, Cook ER, Krusic PJ, *et al.* 2003. Tests of the RCS method for preserving low-frequency variability in long tree-ring chronologies. *Tree-Ring Res* **59**: 81–98.

Osborn TJ, Briffa KR, and Jones PD. 1997. Adjusting variance for sample-size in tree-ring chronologies and other regional-mean time-series. *Dendrochronologia* **15**: 89–99.

Pfister C. 1999. Wetternachhersage. 500 Jahre Klimavariationen und Naturkatastrophen (1496–1995). Bern, Switzerland; Stuttgart, Germany; Wien, Austria: Verlag Paul Haupt.

Wigley TML, Briffa KR, and Jones PD. 1984. On the average of value of correlated time series, with applications in dendroclimatology and hydrometeorology. *J Clim Appl Meteorol* **23**: 201–13.

